

Quantized Vortex States of Strongly Interacting Bosons in a Rotating Optical Lattice

Rajiv Bhat¹, B. M. Peden¹, B. T. Seaman¹, M. Krämer¹, L. D. Carr² and M. J. Holland¹

¹*JILA and Department of Physics, University of Colorado at Boulder, CO 80309-0440, USA*

²*Physics Department, Colorado School of Mines, Golden, Colorado 80401, USA*

Bose gases in rotating optical lattices combine two important topics in quantum physics: superfluid rotation and strong correlations. In this paper, we examine square two-dimensional systems at zero temperature comprised of strongly repulsive bosons with filling factors of less than one atom per lattice site. The entry of vortices into the system is characterized by jumps of 2π in the phase winding of the condensate wavefunction. A lattice of size $L \times L$ can have at most $L - 1$ quantized vortices in the lowest Bloch band. In contrast to homogeneous systems, angular momentum is not a good quantum number since the continuous rotational symmetry is broken by the lattice. Instead, a quasi-angular momentum captures the discrete rotational symmetry of the system. Energy level crossings indicative of quantum phase transitions are observed when the quasi-angular momentum of the ground-state changes.

I. INTRODUCTION

Rotating Bose-Einstein condensates in dilute alkali gases provide a rich playground for the study of quantized vortices in superfluid systems. One major advantage is the ability to directly image vortex cores and study their static and dynamic properties. Vortices, first made by quantum state engineering of condensate wave functions [1, 2], are typically now produced by mechanical stirring of ultracold atomic clouds [3, 4]. Remarkable images of large vortex lattices containing more than one hundred vortices in an Abrikosov type triangular configuration have produced striking evidence for the superfluidity of Bose-Einstein condensed alkali gases [5, 6].

Employing the analogy between the Hamiltonian for a two-dimensional electron gas in a strong magnetic field and that for a rotating atomic gas, it has been pointed out that the physics of the fractional quantum Hall effect (FQHE) should emerge when the number of vortices and the number of atoms become comparable [7, 8, 9, 10]. Achieving this regime experimentally is a significant goal of the field at this time. One of the reasons for this is the connection with many problems of interest in condensed matter systems where strongly correlated electron effects have been discussed and studied. The direct approach of spinning-up a Bose-Einstein condensate to reach the regime of strongly correlated effects is difficult because of the need to reach a parameter regime of low particle number per vortex and extremely low temperature [11]; for this reason the FQHE regime has yet to be achieved with cold atoms.

Ultracold gases are typically dilute, and the interaction effects can be well incorporated by perturbation theory. However, it is possible to manipulate and enhance the interaction effects in a number of ways so that the perturbative treatment fails. One possibility is to increase the two-body scattering length via a Feshbach resonance. An alternative method is to modify the effective interactions through application of an optical lattice. An optical lattice is formed from an off-resonant light intensity pattern created by the interference of several laser beams. The

atoms feel a potential proportional to the intensity of the light field. As the laser fields are made more intense, the interactions are enhanced because the atoms become more strongly confined in the lattice wells. This technique was exploited in the theoretical and experimental study of the Mott-insulator to superfluid quantum phase transition in a non-rotating system [12, 13]. Theoretical studies have been done linking the Hofstadter butterfly [14] and the FQHE [15, 16] with bosons in an optical lattice in the presence of an effective magnetic field.

It is thus a natural question to pose as to whether one can combine the intriguing physics of the rotating gas with the enhanced interactions in an optical lattice. The motivation would be to move the regime of quantum Hall physics towards a parameter space that is experimentally achievable. In a first experiment with a rotating optical lattice, Tung *et al.* [17] have recently demonstrated vortex pinning in a weakly interacting BEC. This was realized by passing a laser beam through a mask that contains holes arranged in a particular configuration and then focusing the laser beams to form the lattice interference pattern. The two dimensional optical lattice is rotated by spinning the mask.

In this paper, we formulate a theoretical description of bosons in rotating optical lattices and illuminate the connections with vortex physics, building upon results presented in an earlier article [18]. Certain aspects of this problem such as single vortex formation [19] and vortex pinning [20] have been theoretically explored for high filling factors (large number of atoms per site). Burkov *et al.* [21] have shown the formation of delocalized vortex clusters in lattices containing superfluids in the presence of an *effective* magnetic field created by modulating the optical lattice. We consider strongly repulsive bosons in a small 2D rotating square optical lattice with filling factors less than unity. In this regime, exact solutions are tractable and indicate key properties of larger systems.

The system can be studied using a modified Bose-Hubbard Hamiltonian with a complex, site-dependent hopping term which is sufficient to describe physics in the lowest Bloch band. The lattice breaks the continuous rotational symmetry associated with the angular momen-

tum operator. Instead, it possesses a discrete rotational symmetry, and the generator of this discrete rotation, the quasi-angular momentum, plays an important role. The square lattice is four-fold rotationally symmetric and the quasi-angular momentum operator generates rotations in steps of $\pi/2$.

The entry of vortices into the system is marked by 2π jumps in the phase winding of the condensate wavefunction. We show that a maximum vorticity of $2\pi(L-1)$ is possible for the lowest band in a lattice of size $L \times L$. Changes in the quasi-angular momentum of the ground state are associated with energy level-crossings as a function of changing angular velocity. For filling commensurate with the symmetry of the system, the quasi-angular momentum is zero at all angular velocities. In this case, avoided energy level crossings of the ground-state are observed as a function of lattice angular velocity. For incommensurate filling, there are energy level crossings for many particles at zero temperature. Since these correspond to a symmetry change in the ground state as a function of a Hamiltonian parameter at zero temperature, and the property holds for systems of arbitrary size and particle number, these critical points are *quantum phase transitions* [27].

This paper is structured as follows. Section II provides the theoretical framework by sketching the derivation of a modified Bose-Hubbard Hamiltonian for describing lowest-band physics and discusses its regime of validity, along with the principal observables. Section III describes general characteristics of the system such as the Mott-insulator/superfluid phase diagram and the effect of strong repulsive interactions. The behavior of the density distribution as a function of rotation is illustrated. Section IV presents a characterization of the quasi-angular momentum. Sections V and VI discuss results for a single particle and many particles in the system, respectively. Section VII summarizes the main results of this paper.

II. MODIFIED BOSE-HUBBARD HAMILTONIAN FOR ROTATING LATTICES

A. Hamiltonian

The energy for a fixed number of bosons in an optical lattice can be broken down into three components corresponding to the kinetic energy, the potential energy due to the lattice, and the interaction energy between bosons. Using a standard procedure [22], the Hamiltonian in the reference frame rotating with angular velocity Ω about the z -axis is $\hat{H} = \hat{H}_0 - \int d\mathbf{x} \hat{\Phi}^\dagger \Omega L_z \hat{\Phi}$, where \hat{H}_0 is the Hamiltonian in the laboratory frame and L_z is the angular momentum. This coordinate transformation facilitates the calculation of the ground state in the laboratory frame since it renders the Hamiltonian time-independent.

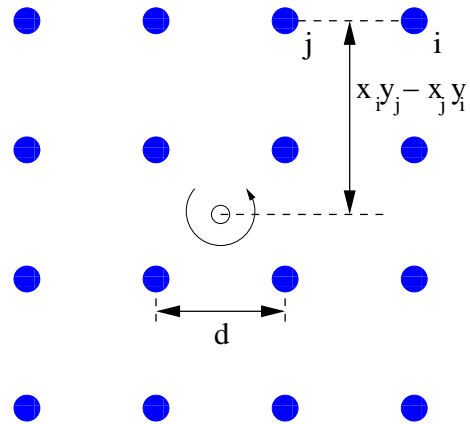


FIG. 1: Schematic for a 4×4 lattice rotating in the counter-clockwise direction. Sites labeled i and j are nearest neighbors. The rotation-driven hopping between neighbouring sites is governed by the parameter $K_{ij} = \beta(x_i y_j - x_j y_i)/d$ where β is given by the overlap integral Eq. (8) and the second factor is the perpendicular distance of the line joining the two neighboring sites from the center of rotation.

The Hamiltonian in the rotating frame reads

$$\hat{H} = \int d\mathbf{x} \hat{\Phi}^\dagger \left[-\frac{\hbar^2}{2M} \nabla^2 + V^{\text{lat}}(\mathbf{x}) + \frac{g}{2} \hat{\Phi}^\dagger \hat{\Phi} - \Omega L_z \right] \hat{\Phi}, \quad (1)$$

where M is the single particle mass and g is the coupling constant for repulsive two-body scattering in a dilute gas. The bosonic field operator $\hat{\Phi}$ obeys the commutation relationship $[\hat{\Phi}(\mathbf{x}), \hat{\Phi}(\mathbf{x}')^\dagger] = \delta(\mathbf{x} - \mathbf{x}')$. Particles can be described using an orthonormal Wannier basis $W_i^{(p)}(\mathbf{x})$. Here, i indexes the N sites on the lattice and p denotes the band index [12]. If the energy due to interaction and rotation is small compared to the energy separation between the lowest and first excited band, the particles are confined to the lowest Wannier orbital. We shall consider this regime only and henceforth will drop the band index p . The field operator $\hat{\Phi}$ can be expanded in terms of this Wannier basis, $W_i(\mathbf{x})$, and the corresponding site-specific annihilation operators, \hat{a}_i , as

$$\hat{\Phi}(\mathbf{x}) = \sum_{i=1}^N \hat{a}_i W_i(\mathbf{x}). \quad (2)$$

Alternatively, a rotation dependent phase can be ascribed to each Wannier basis element and the field operator $\hat{\Phi}$ expanded accordingly. Comparisons with this approach are made in the next subsection.

In the tight binding regime, tunneling between sites which are not nearest neighbors can be neglected. The interaction between particles on nearest neighbor sites can also be neglected. Using this approximation and substituting Eq. (2) into Eq. (1) yields the modified Bose-

Hubbard Hamiltonian

$$\hat{H} = -t \sum_{\langle i,j \rangle} (\hat{a}_i^\dagger \hat{a}_j + \hat{a}_i \hat{a}_j^\dagger) + \epsilon \sum_i \hat{n}_i + \frac{U}{2} \sum_i \hat{n}_i (\hat{n}_i - 1) - i\hbar\Omega \sum_{\langle i,j \rangle} K_{ij} (\hat{a}_i^\dagger \hat{a}_j - \hat{a}_i \hat{a}_j^\dagger), \quad (3)$$

where i and j are site indices, $\langle i, j \rangle$ indicates that the sum is over nearest neighbors, and \hat{n}_i is the number operator for site i . The first three terms are common to the well-studied Bose-Hubbard Hamiltonian for particles in a stationary lattice [23]. The parameters t and ϵ are integrals describing hopping and onsite zero-point energy respectively:

$$t \equiv \int d\mathbf{x} W_i^*(\mathbf{x}) \left[-\frac{\hbar^2}{2M} \nabla^2 + V^{(lat)}(\mathbf{x}) \right] W_j(\mathbf{x}), \quad (4)$$

$$\epsilon \equiv \int d\mathbf{x} W_i^*(\mathbf{x}) \left[-\frac{\hbar^2}{2M} \nabla^2 + V^{(lat)}(\mathbf{x}) \right] W_i(\mathbf{x}). \quad (5)$$

Wannier functions along the x and y directions can be decoupled for a square lattice, and accordingly, the integrals become one-dimensional. The third term in the Hamiltonian, Eq. (3), describes the interaction between particles on the same site. For an s -wave scattering length a_s [12, 24],

$$U \equiv \frac{4\pi a_s \hbar^2}{M} \int d\mathbf{x} |W_i(\mathbf{x})|^4. \quad (6)$$

The last term in Eq. (3) is the modification due to the rotation and favors hopping along one azimuthal direction. K_{ij} is a product of the azimuthal overlap integral, β , which is dependent on the geometry and form of the lattice, and the perpendicular distance of the line joining sites i and j from the center of rotation (Fig. 1),

$$K_{ij} = \frac{\beta}{d} (x_i y_j - x_j y_i). \quad (7)$$

Here, (x_i, y_i) are the coordinates of the i^{th} site with the origin located at the center of rotation. The lattice spacing is d and

$$\beta \equiv \int dx W_i^*(x-d) \partial_x W_j(x) \quad (8)$$

We numerically calculate t and β for a sinusoidal lattice potential, $V = V_0(\sin^2(\pi x/d) + \sin^2(\pi y/d))$ using Mathieu functions. The results are plotted in Fig. 2 as a function of the lattice depth up to a very tight confinement of $V_0/E_R = 20$, with $E_R = \hbar^2 \pi^2 / 2md^2$ denoting the recoil energy.

The eigenstates of the Hamiltonian can be written in the form

$$|\Psi\rangle = \sum_{\{n_i\}} c_{\{n_i\}} |n_1, n_2, \dots, n_N\rangle. \quad (9)$$

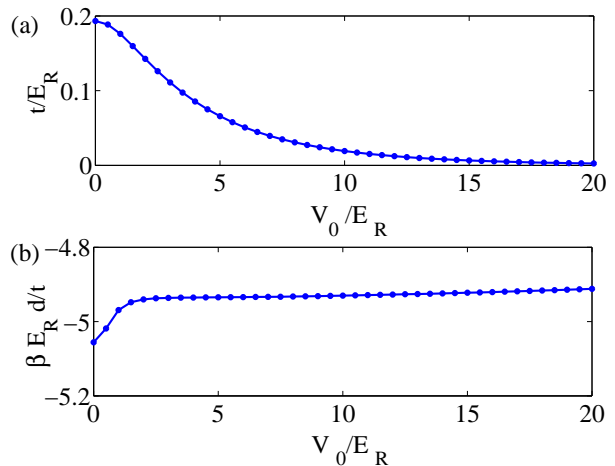


FIG. 2: Overlap integrals t (Eq. (4)) and β (Eq. (8)) for a standing wave optical lattice described by $V = V_0(\sin^2(\pi x/d) + \sin^2(\pi y/d))$. The lattice depth is given in units of the recoil energy $E_R = \hbar^2 \pi^2 / 2md^2$. (a) The hopping parameter t decreases exponentially as a function of V_0 . (b) $\beta d E_R / t$ as a function of lattice depth. In the tight-binding regime, βd scales roughly linearly with t/E_R . In this paper we use $\beta = 4.93t/E_R d$ and $t = 0.02E_R$, corresponding to a standing wave optical lattice of depth $V_0/E_R = 10$.

Here N indicates the total number of sites and $\{n_i\}$ indicates the set of all possible products of number states constrained by the total number of particles, i.e. $\sum_i n_i = n$. In this paper, we use the truncated set of Fock states $\{|0\rangle, |1\rangle\}$ to describe the number of particles at each site [16, 25]. This corresponds to assuming a regime of strong repulsive interactions, i.e., that of hard-core bosons. Note that in a 1D lattice this approach is equivalent to mapping bosonic operators onto fermionic ones via the Jordan-Wigner transformation [26, 27]. A test of the regime of validity of this approximation is provided in Section III A. The Hamiltonian is constructed using this basis and diagonalized to find the ground state energy eigenvalue and eigenstate. A set of tools, which are described in Section II C, are then used to analyze the ground state. Note that solving for the Hamiltonian in Eq. (3) is equivalent to putting the 2D lattice inside a box with infinite potential walls. This effect leads to a number density distribution that is peaked in the center for zero rotation.

B. Regime of Validity of the Hamiltonian

Many aspects of studying the characteristics of bosons in a rotating optical lattice map onto the extensively studied problem of Bloch electrons in the presence of a magnetic field [28, 29, 30, 31]. This subsection makes a connection with the electron problem, while exploring, in parallel, the limitations of using the lowest band Bose-

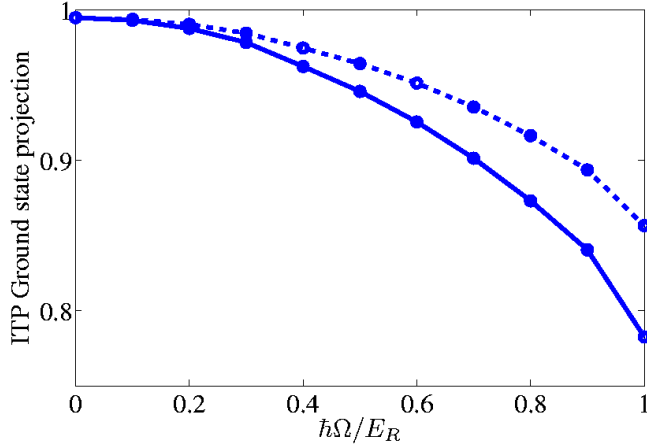


FIG. 3: Projection of the ground state obtained using imaginary time propagation (ITP) onto the Hilbert space spanned by the eigenvectors obtained using \hat{H} (solid line) (Eq. (3)) and \hat{H}_2 (dashed line) (Eq. (11)) for a 2×2 lattice with a lattice depth of $V_0 = 10E_R$. Ω is in units of the recoil energy. The overlap is good even up to $\Omega = E_R/\hbar \sim 50t$ where t is the hopping energy.

Hubbard Hamiltonian.

The Hamiltonian described in Eq. (3) only takes into account Wannier orbitals from the lowest band—an excellent approximation for small Ω and a deep lattice. An alternative formulation can be obtained by using Eq. (1) in conjunction with a different Wannier basis given by

$$W'_i(\mathbf{x}) = \exp\left[-\frac{iM}{\hbar} \int_{\mathbf{x}_i}^{\mathbf{x}} \mathbf{A}(\mathbf{x}') \cdot d\mathbf{x}'\right] W_i(\mathbf{x}), \quad (10)$$

resulting, for the case of a single particle in which interaction effects are not present, in the following Hamiltonian,

$$\begin{aligned} \hat{H}_2 = & - \sum_{\langle i,j \rangle} \left(t + \frac{1}{2} m \Omega^2 t' \right) \hat{a}_i^\dagger \hat{a}_j \\ & \times \exp\left[-\frac{im}{\hbar} \int_{\mathbf{x}_j}^{\mathbf{x}_i} \mathbf{A}(\mathbf{x}') \cdot d\mathbf{x}'\right] + h.c. \end{aligned}$$

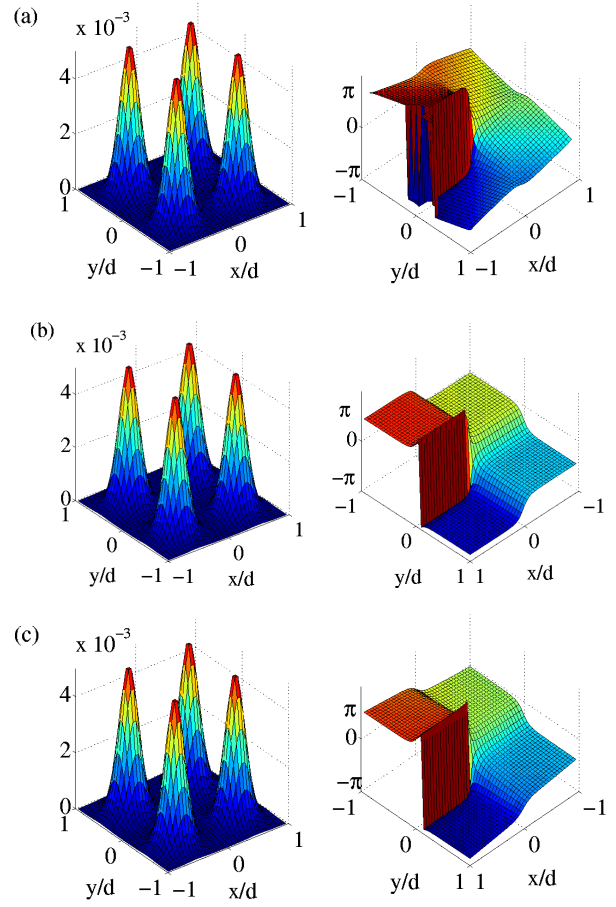


FIG. 4: Spatial ground state number density (left) and phase information (right) for one particle in a 2×2 sinusoidal lattice with $\Omega = 0.5E_R/\hbar$ and $V_0 = 10E_R$ obtained using (a) Imaginary time propagation, (b) Hamiltonian \hat{H}_1 (Eq. (3)) and (c) Hamiltonian \hat{H}_2 (Eq. (11)).

$$+ \sum_i \left(\epsilon - \frac{1}{2} m \Omega^2 r_i^2 - \frac{1}{2} m \Omega^2 \epsilon' \right) \hat{a}_i^\dagger \hat{a}_i. \quad (11)$$

Here, t' and ϵ' refer to integrals similar to those defined for t and ϵ in Eqs. (4) and (5). $\mathbf{A}(\mathbf{x}) = \boldsymbol{\Omega} \times \mathbf{x}$ is the analog of the magnetic vector potential. For more than one particle, this Hamiltonian must be extended to include the effects of interactions. Note that \hat{H}_2 and $W'_i(\mathbf{x})$ have forms similar to those used traditionally in the treatment of Bloch electrons in the presence of magnetic fields. A similar formulation has also been used to study bosons in an optical lattice in the presence of an effective magnetic field [14, 15] and for bosons in a rotating optical lattice [19].

In this subsection, the two approaches are compared with results for a single particle obtained from imaginary time propagation (ITP) for one particle in a 2×2 lattice. This analysis gives rise to three findings: (1) The ground state of the Hamiltonian described in Eq. (3) no longer depends on the increase in Ω once a maximum

phase difference of $\pi/2$ between neighboring sites has been reached, i.e., all the vortex entry transitions possible within the lowest band have occurred. For one particle in a 2×2 lattice, the corresponding maximum phase winding is 2π . This limitation does not apply to the Hamiltonian Eq. (11). (2) The Hilbert spaces spanned by the eigenstates of both Hamiltonians Eq. (3) and Eq. (11) capture most of the exact ground state wavefunction for $\hbar\Omega \leq E_R$. Note that $\hbar\Omega \sim E_R$ is large from an experimental point of view. For the case of one particle in a 2×2 lattice, the projection of the exact wavefunction on either Hilbert space is $\geq 90\%$ for $\hbar\Omega \sim 0.5E_R$ (Fig. 3). Both approaches yield accurate density profiles for large Ω ($\sim E_R/\hbar$) but differ from the ITP-result, and from each other, with regard to the velocity pattern. Note that \hat{H} and \hat{H}_2 involve different approximations to the phase gradient. The Hamiltonian \hat{H} allows for phase changes only in the region of overlap of next-neighbor Wannier functions $W_i(\mathbf{x})$, i.e., yields a uniform phase around the site center (Fig. 4(b)). The Hamiltonian \hat{H}_2 requires phase gradients to be proportional to Ω and allows for non-zero phase gradients within each well (Fig. 4(c)). (3) The lattice rotation frequencies at which the first vortices appear, as will be discussed later, are slightly different in the two cases over the range of interest due to the different influence of higher bands in the three formulations. The remainder of our work is primarily concerned with the states of the system at low Ω and since these are well captured by the simpler lowest band Hamiltonian described in Eq. (3), we use it for the rest of the paper.

C. Toolkit

We evaluate six quantities to characterize the behavior of the system: (1) energy, (2) site number density, (3) intersite current in the rotating frame, (4) average angular momentum, (5) quasi-angular momentum eigenvalues and (6) phase winding of the condensate wavefunction.

The ground state energy is obtained as the lowest eigenvalue of the Hamiltonian. The site number density is the expectation value of the number operator: $n_i = \langle \hat{a}_i^\dagger \hat{a}_i \rangle$. The expectation value for the current J_{ij} flowing from site i to a neighboring site j in the rotating frame is obtained using the continuity equation,

$$\begin{aligned} J_{ij} &= -\frac{1}{i\hbar} \langle [\hat{n}_i, \hat{H}_{ij}] \rangle \\ &= \frac{it}{\hbar} \langle \hat{a}_i \hat{a}_j^\dagger - \hat{a}_i^\dagger \hat{a}_j \rangle - \Omega K_{ij} \langle \hat{a}_i \hat{a}_j^\dagger + \hat{a}_i^\dagger \hat{a}_j \rangle, \end{aligned} \quad (12)$$

where the current is in units of t/\hbar . \hat{H}_{ij} in Eq. (12) is the part of the Hamiltonian operator relevant to sites i and j . Since the number density on any site i is constant for any steady state solution, the algebraic sum of currents associated with any site i is zero.

The derivative of the energy with respect to the angular velocity Ω — keeping all other Hamiltonian param-

eters constant — gives direct access to the average angular momentum,

$$\langle \hat{L}_z \rangle = -\frac{\partial E}{\partial \Omega}. \quad (13)$$

Quasi-angular momentum is calculated based on the four-fold rotational symmetry in the Hamiltonian created by the square lattice, i.e., rotating the system by 90 degrees has no effect on the Hamiltonian. This is discussed in detail in Section IV. Here, we give a brief description of the way we calculate the quasi-angular momentum. A discrete rotational symmetry operator, $\mathbf{R}(\pi/2)$, can be constructed such that $\mathbf{R}(\pi/2)$ acting on a wavefunction rotates that wavefunction by ninety degrees. $\mathbf{R}(\pi/2)$ commutes with the Hamiltonian and therefore shares simultaneous eigenfunctions. Applying this operator four times corresponds to a rotation of 2π , bringing the wavefunction back to its original state:

$$\begin{aligned} \mathbf{R}\Psi &= r\Psi \\ \mathbf{R}^4\Psi &= \Psi \Rightarrow r = e^{im\pi/2}, \quad m \in \{0, 1, 2, 3\}. \end{aligned} \quad (14)$$

Hence, the eigenvalues of $\mathbf{R}(\pi/2)$ are defined by the quantized dimensionless quasi-angular momentum m . From an operational standpoint, we apply a rotation $\mathbf{R}(\pi/2)$ to Ψ and read out the eigenvalue, r . Note that the discrete rotational symmetry operator can be generalized to a n -fold rotationally symmetric system.

The condensate wavefunction is the eigenfunction corresponding to a macroscopically large eigenvalue of the one-body density matrix $G^{(1)}$, with all other eigenvalues being non-macroscopic [32, 33]. In usual tensor notation, $G_{ij}^{(1)} = \langle \hat{a}_j^\dagger \hat{a}_i \rangle$. The phase of the condensate wavefunction describes the superfluid properties of the system. In the small systems we consider in this paper, this is not a rigorous definition. However, a meaningful condensate wavefunction can still be obtained in this way since in the superfluid regime one of the eigenvalues of the one-body density is always significantly larger than all the others, even for a very small number of particles. The phase winding around the perimeter of the condensate wavefunction, Θ_{cf} , when divided by 2π gives the vorticity of the system. The subscript cf indicates that the phase winding refers to that of the condensate wavefunction.

III. GENERAL CHARACTERISTICS

This section describes four general features of bosons in rotating lattices: (1) interaction effects, (2) the Mott insulator/superfluid quantum phase diagram for the system, (3) number density depletion at the center for odd lattices, and (4) number density distribution for even lattices. The first subsection lays out the justification for our choice of studying lattices using a truncated Fock space as mentioned above in connection with Eq. (9). The second subsection connects with existing understanding of the phase diagram for the Bose-Hubbard

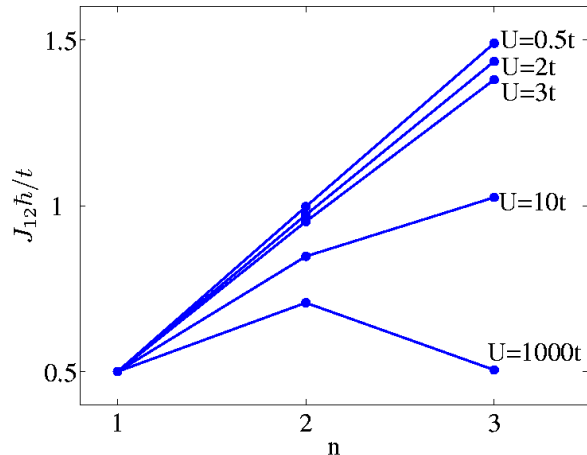


FIG. 5: Current J_{12} between adjacent sites of a 2×2 unit cell lattice as a function of total number of particles n for different values of the ratio between repulsive interaction and hopping U/t at large rotation ($\hbar\Omega \sim 0.6E_R \gg t$). For weak interaction, $U = 0.5t$, the particles can freely cross each other and the current is proportional to the number of particles. As the interaction increases, the current per particle drops as a function of filling. For $U = 1000t$, the current for three particles is the same as that for one particle, indicating a particle-hole symmetry. The current was evaluated using a four-state Fock basis on each site, which allowed three particles per site.

model. The third subsection discusses our choice of lattices with an even number of sites and the last describes number density rearrangement with vortex entry.

A. Effect of interaction

Interaction between bosons inhibits current flow by making it difficult for particles to cross each other. To demonstrate this we consider currents in a 2×2 unit lattice using a four-state Fock basis on each site. Figure 5 is a plot of the current in the rotating frame between two neighboring sites as a function of filling for different interaction strengths at fixed angular velocity ($\hbar\Omega \sim 0.6E_R \gg t$). For weak interactions ($U = 0.5t$), the current is proportional to the number of particles as they can flow independently of each other. However, the current per particle drops with increasing interaction and filling. At large interaction ($U = 1000t$), the current for three particles (one hole) is the same as for one particle in the system. This particle-hole symmetry is characteristic of the regime where bosons are impenetrable, i.e., of the regime where the two-state approximation applies [16, 25]. In fact, currents calculated for $U \geq 100t$ using the two-state approximation coincide with those obtained with a larger Fock space. The main results of this paper are obtained assuming the atoms to be impenetrable and hence are expected to be quantitatively

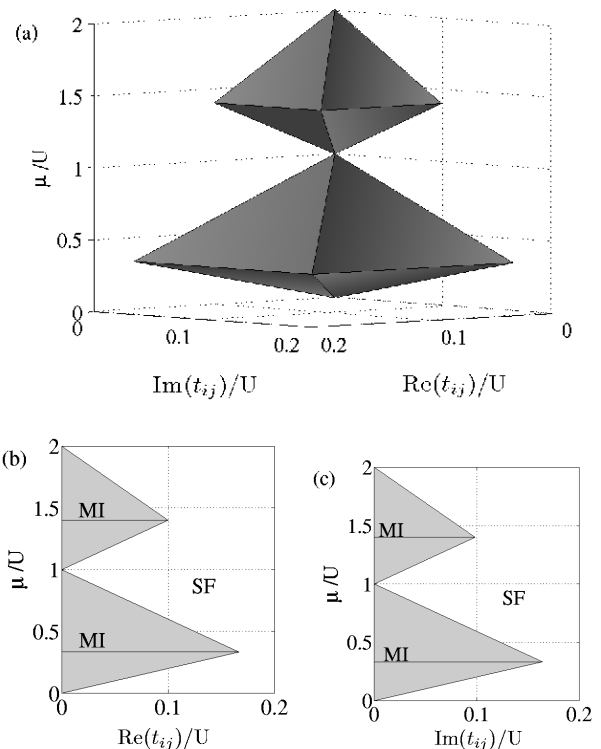


FIG. 6: (a) Mott-Insulator zone boundaries for bosons in a 2×2 lattice as a function of chemical potential μ and of the real and imaginary parts of the complex hopping parameter described in Eq. (16). The volume inside the shaded surfaces corresponds to Mott-insulating states with average fillings of one and two particles per site in the lower and upper volume respectively. (b) The $x-z$ cross-section of the phase diagram is the same as that obtained using the Bose-Hubbard Hamiltonian for a non-rotating system. (c) The $y-z$ cross section of the phase diagram is similar to the $x-z$ cross section. Note that the shape of the Mott zones will change on going beyond the two-state approximation [34].

accurate in the regime $U \geq 100t$ for fillings ≤ 1 .

B. Phase diagram

The phase diagram for the non-rotating Bose-Hubbard model is obtained in the grand-canonical ensemble by adding a term $-\mu \sum_i \hat{n}_i$ to the Hamiltonian. The phase diagram separates into two regions—the Mott insulator (MI) lobes with commensurate filling (integer number of atoms per site) and the superfluid (SF) regions with incommensurate filling. The phase diagram for the non-rotating lattice was first studied in Ref. [23].

The introduction of rotation makes the hopping energy parameter t complex and site-dependent as can be seen by rewriting Eq. (3) in the grand canonical description

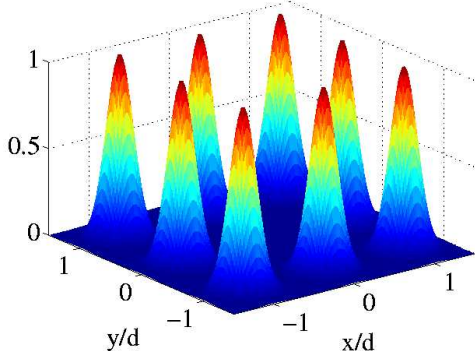


FIG. 7: Number density distribution for one particle in a 3×3 lattice of depth $V_0 = 10E_R$ at a lattice rotation of $\hbar\Omega = E_R$. There is almost complete number depletion in the central site because it coincides with the center of rotation and hence the vortex core.

after combining the first and last terms.

$$\hat{H} = -\sum_{\langle i,j \rangle} \left(t_{ij} \hat{a}_i^\dagger \hat{a}_j + t_{ij}^* \hat{a}_i \hat{a}_j^\dagger \right) + (\epsilon - \mu) \sum_i \hat{n}_i + \frac{U}{2} \sum_i \hat{n}_i (\hat{n}_i - 1), \quad (15)$$

$$t_{ij} = t + i\hbar\Omega K_{ij}. \quad (16)$$

The surface in Fig. 6 represents the boundary between the Mott insulator (MI) and superfluid (SF) regions as a function of the chemical potential and of the real and imaginary parts of the hopping parameter t_{ij} . The zero point energy ϵ in each well has been set to zero since it gives rise to an irrelevant overall shift. Note that the shape of the tip of the Mott zones in Fig. 6 differs slightly if more than two Fock states are used to represent each state [34]. At $\Omega = 0$ ($\text{Im}(t_{ij}) = 0$, Fig. 6(b)), the phase boundary matches that for the non-rotating Bose-Hubbard model in the two-state approximation. A similar diagram is obtained when setting $\text{Re}(t_{ij}) = 0$ (Fig. 6(c)). In general, this similarity need not be present for larger systems where t_{ij} is not the same for all pairs of nearest neighbors as in the example of a 2×2 lattice. Note that even though $\text{Im}(t_{ij})$ can be varied freely via Ω for a given t and non-zero K_{ij} , the reverse is not true. This is because for a particular realization of a lattice, the two overlap integrals t (Eq. (4)) and β (Eq. (8)) are both fixed by the lattice depth. Hence, a fixed $\text{Im}(t_{ij}) = \Omega K_{ij}$ implies a fixed $\text{Re}(t_{ij}) = t$. In the case of a standing wave optical lattice in the tight binding regime, K_{ij} is approximately proportional to t/E_R (see Fig. 2). This makes the plane $\text{Re}(t_{ij}) = 0$ of the phase diagram inaccessible.

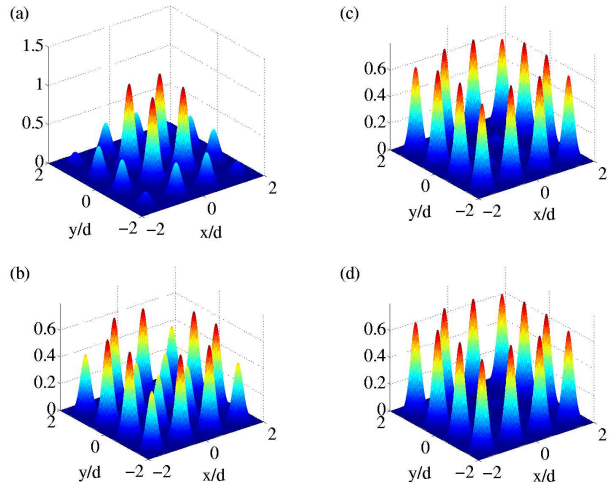


FIG. 8: Number density distribution for one particle in a 4×4 lattice at $V_0 = 10E_R$. (a) $\hbar\Omega = 0.1E_R$ - rotation has yet to enter the system. The center-peaked distribution is due to the infinite potential walls at the perimeter of the lattice. (b) $\hbar\Omega = 0.2E_R$ (c) $\hbar\Omega = 0.4E_R$ (d) $\hbar\Omega = 0.8E_R$. At large rotation, particles get pushed to the outermost sites creating a washing machine effect.

C. Differences between even and odd lattices

In the study of rotating lattices, the position of the center of rotation gives rise to an important distinction between two kinds of lattices: lattices with an even number of sites (e.g., 2×2 , 4×4) and lattices with an odd number of sites (e.g., 3×3 , 5×5). If assumed to be at the center of the system, the axis of rotation passes through a peak in the lattice potential in the case of even lattices while it passes through the central site for odd lattices. It is useful to briefly touch upon two interesting aspects of the ground state solution for odd lattices: (1) there is nearly complete number density depletion in the center site when rotation enters the system, as would be expected at the vortex core in a continuous system (Fig. 7); and (2) there are no currents along the radial direction ($K_{ij} = 0$) so that particles only hop along the azimuthal direction. Even lattices have no sites which are nearest neighbors in a strictly radial direction, but the main results for particles in a rotating even lattice can be mapped onto those for particles in an odd lattice. Only the even lattice is discussed for the rest of the paper since it captures the most important physical features.

D. Number density distribution

The number density distribution is obtained by evaluating the expectation of the site-specific number operator \hat{n}_i . Figure 8 describes the number distribution for one particle in a 4×4 lattice with phase windings of 0 , 2π , 4π , and 6π . For small angular velocities, there is no

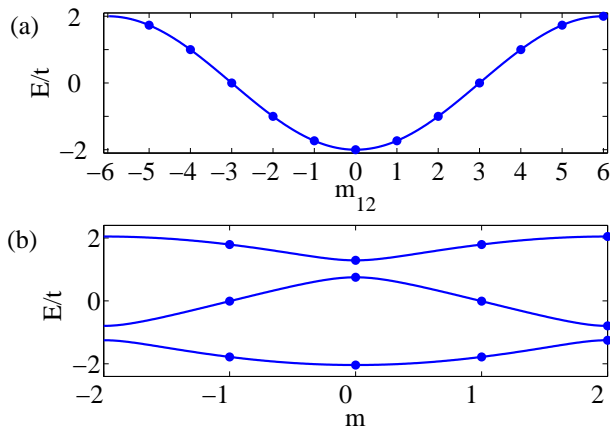


FIG. 9: (a) Energy-quasi angular momentum dispersion relationship for a 12-site ring. Positive and negative m_{12} values indicate rotation in opposite directions. The velocity of the particles in any state is given by the slope of the dispersion curve at the point. Accordingly, the velocity is maximum at $m = 3$ (b) Energy—quasi-angular momentum dispersion relationship for a 12-site ring with a small four-fold periodic potential. Note the lines joining states are obtained by extrapolating for an infinite system.

effect of rotation on the ground state of the system and the number density is center-peaked (Fig. 8(a)). In the continuous limit of the lattice spacing becoming infinitesimal, this mirrors the number distribution for particles in a 2D box with infinite potential walls. The distribution changes each time a vortex enters the system. For large rotation (Fig. 8d), we observe a *washing machine effect*, as the number density gets concentrated at the perimeter. The inner sites have a small non-zero number density in this limit.

IV. QUASI-ANGULAR MOMENTUM

The presence of the lattice breaks the continuous rotational symmetry of the system. The eigenvalues of the angular momentum operator are therefore no longer good quantum numbers because the rotational symmetry associated with \hat{L} has been replaced with a discrete rotational symmetry. In this section, ideas of discrete translational symmetry and Bloch's theorem are mapped onto a discrete rotational symmetry problem to generate quasi-angular momentum states. Exact results are presented for the modified Bose-Hubbard model in the context of a single particle one-dimensional ring, and connections are made with the square lattice.

Consider a one-dimensional lattice with periodic boundary conditions, i.e., a ring lattice of N sites. A rotation of $2\pi/N$ leaves the system invariant and hence the rotation operator $R(2\pi/N)$ commutes with the Hamiltonian. This is also true for a square ring because the site dependent parameter K_{ij} in the Hamiltonian (Eq. (3))

depends on the perpendicular distance of the line connecting two nearest neighbor sites from the center of rotation. The energy eigenstates can be labeled using the eigenvalues of $R(2\pi/N)$:

$$R(2\pi/N)|m\rangle = e^{i2\pi m/N}|m\rangle : m \in \{0, \dots, N-1\}, \quad (17)$$

where the exact eigenvectors shown can easily be derived by expanding $|m\rangle$ in the Fock basis and demanding periodic boundary conditions.

At this point, it is useful to make a connection with conventional Bloch theory. $R(\pi/2)$ is analogous to the discrete translation operator $\mathbf{T}(d)$ for a stationary one-dimensional lattice of period d [35],

$$\mathbf{T}(d)\Psi(x_1, \dots, x_n) = e^{iqd}\Psi(x_1, \dots, x_n), \quad (18)$$

where $\Psi(x_1, \dots, x_n)$ is an eigenfunction of the translation operator. The eigenvalues of $\mathbf{T}(d)$ are described by the quasi-momentum q . In a way exactly analogous to that of quasi-momentum Bloch states for a discrete translation operator, we can identify these m -values in Eq. (17) as quasi-angular momenta. Note that this discussion so far is completely general and applies to both the single-particle and many-particle cases.

To illustrate the role of the quasi-angular momentum and the connection with the quasi-momentum in systems with discrete translational symmetry, consider one particle in a 12 site static ring. Each of the sites is indexed by an azimuthal coordinate, ϕ_i . The energy spectrum takes on the well-known dispersion relation observed for the lowest Bloch band of a particle in a 1D lattice with periodic boundary conditions in the tight-binding regime (Fig. 9(a)). Since the system has 12-fold symmetry, the quasi-angular momentum, m , can take on 12 possible values. The slope of the energy plot provides the velocity of the particle. As discussed before (Section II), rotation is introduced by adding a term, $-(\hbar\Omega/i)\partial_\phi$, to the Hamiltonian in order to obtain the ground state in rotating frame coordinates. As Ω is ramped in a particular direction, the ground state quasi-angular momentum changes from $m = 0$ to $m = 3$ in steps of 1 (not shown here). The $m = 3$ state corresponds to the maximum slope of the dispersion and the largest particle velocity. A particle in the $m = 4$ state has the same velocity as the $m = 2$ state but with a higher energy. Quasi-angular momenta $m = 7, \dots, 11$ correspond to $m = -5, \dots, -1$ and describe circulation in the opposite direction. This is described by the C_{12} point symmetry group.

Consider now a 12-site ring perturbed by a four-fold symmetric periodic potential. The Hamiltonian, $H = H_{12} + V$, is the sum of two terms, the 12-site Hamiltonian H_{12} which has a 12-fold rotation symmetry and a potential V which has a four-fold rotation symmetry. Figure 9(b) is the energy dispersion relation as a function of quasi-angular momentum for the 12-site lattice ring with this small four-fold symmetric potential. Since the potential increases the rotational symmetry from $d = 2\pi/12$ to $d = 2\pi/4$, the Brillouin zone is narrowed down to

$m = -2, \dots, 2$. Three energy bands are created in place of one. States on adjacent bands with the same m value — for example $m_{12} = -2$ and $m_{12} = 2$ — are mixed by the four-fold symmetric potential V , thereby leading to an energy gap at this m value.

An analogous situation occurs when we try to qualitatively understand the properties of a 4×4 lattice, which has 12 sites on the boundary. We adopt a perturbative approach by breaking the system into two non-interacting 12-site and 4-site rings and considering an interaction between them, i.e., $H = H_{12} + H_4 + V$. The interaction with the four-site ring breaks the 12-fold symmetry of the outer ring, reducing it to a four-fold discrete rotational symmetry.

The above example illustrates that a particle in a square lattice is characterized by a four-fold discrete rotational symmetry. The same symmetry considerations hold for many particles in the system. Hence, the many-body eigenstates are quasi-angular momentum states with $m \in \{-2, 1, 0, 1, 2\}$.

In the following we show how the rotation of the lattice leads to a change in quasi-angular momentum in the groundstate of the system in the single-particle case (Section V) and in the many-body case (Section VI). In addition, we show how these transitions affect other properties of the system, such as its average angular momentum and its vorticity.

V. ONE-PARTICLE ANALYSIS

This section examines the response of one particle to lattice rotation. The advantage in first considering only one particle is that it allows one to distinguish general characteristics of the systems from effects due to interaction.

Figure 10 describes the response of the system as a function of the angular velocity Ω . Figures 10(a) and 10(b) show that for increasing Ω the ground state energy in the rotating frame E_0 decreases with discontinuous derivative as different states become energetically favorable. Note that the fact that the eigenstates are not eigenstates of angular momentum is explicitly illustrated here since $\langle L_z \rangle$ takes on non-quantized values.

The abrupt changes in average angular momentum are connected to changes in the quasi-angular momentum m of the groundstate as seen in Fig. 10(c). Since the lattice has four-fold rotational symmetry, the values that the quasi-angular momenta can take on are $m \in \{0, 1, 2, 3\}$. For additional transitions, m repeats itself in behavior analogous to that of *linear quasi-momentum* as one crosses the first Brillouin zone.

The changes in quasi-angular momentum are associated with changes in the phase winding of the single particle wavefunction. The phase winding Θ jumps by 2π each time the quasi-angular momentum of the groundstate changes (Fig. 10(d)). The maximum phase winding of 14π for an 8×8 lattice corresponds to a max-

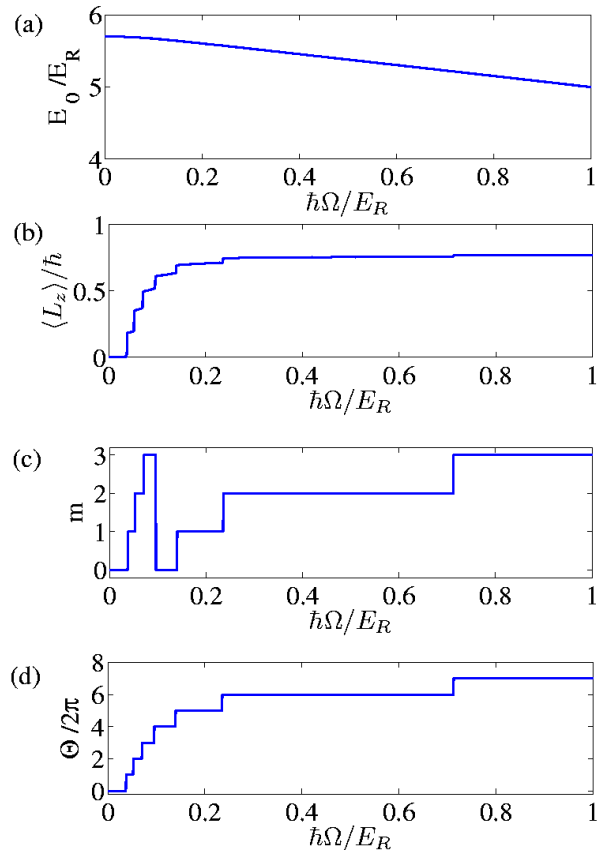


FIG. 10: One particle in an 8×8 lattice. (a) Ground state energy, E_0 vs. Ω . (b) Average angular momentum, $\langle L_z \rangle$ vs. Ω . Note that the expectation value of angular momentum (see Eq. (13)) is not quantized. (c) Quasi-angular momentum m vs. Ω . In direct analogy to quasi-momentum values for linear lattices, m repeats itself. (d) The phase winding, $\Theta/2\pi$, vs. Ω . For the 8×8 lattice, the maximum phase winding is $7 \times 2\pi$.

imum phase difference of $\pi/2$ between any two sites on the lattice boundary. A difference of $\pi/2$ between two lattice sites corresponds to the condition for the maximum current attainable within the lowest band Bose-Hubbard model. This result can be generalized to a lattice of size $L \times L$. The number of sites on the circumference of the lattice is $4(L-1)$ and for a phase difference of $\pi/2$ between two adjacent perimeter sites, the maximum phase winding around the circumference is $2\pi(L-1)$ within the lowest band. Since the notions of an order parameter and of superfluidity do not apply to single particle systems, states with non-zero phase winding can not be referred to as quantized vortices. However, as will be shown in the following, these single particle results extend to many-particle systems in a straightforward manner.

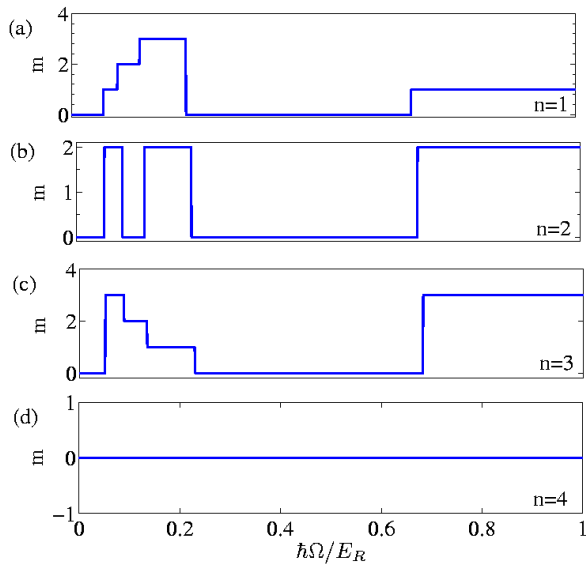


FIG. 11: Quasi-angular momenta for one through four strongly repulsive bosons in a 6×6 lattice. For multiple particles in the lattice and increasing rotation, the quasi-angular momenta cycles through values given by $m = nl \bmod 4$, $l = 0, 1, 2, 3$, where n is the number of particles. (a) $n = 1$: $m = 0, 1, 2, 3, 0, 1$ (b) $n = 2$: $m = 0, 2, 0, 2, 0, 2$ (c) $n = 3$: $m = 0, 3, 2, 1, 0, 3$ (d) $n = 4$: $m = 0$.

VI. MANY-PARTICLE ANALYSIS

This section probes the effects of strongly repulsive interaction when the number of particles in the system is greater than one. The symmetry considerations discussed in Section IV are first tested for many particles. The effect of a symmetry-commensurate filling is explored by considering two different systems - (1) four particles in a 4×4 lattice and (2) five particles in a 4×4 lattice. These two systems correspond to fillings commensurate and incommensurate with the four-fold symmetry of the lattice, respectively.

As discussed in Section IV, the four-fold rotational symmetry allows labeling of the many-body states by their quasi-angular momenta. In a static lattice, the groundstate is always characterized by $m = 0$. This value may change when the lattice is rotated at angular velocity Ω , as has been demonstrated in the single-particle case. In contrast to the single-particle case, the many-body groundstate does not necessarily cycle through all possible m -values as Ω is increased. Instead, the values of quasi-angular momenta it can take on depend on the number of particles. As illustrated in Fig. 11, we see that for n particles in the system, the quasi-angular momentum of the ground state cycles through values satisfying the relation

$$m = nl \bmod 4, \quad (19)$$

where $l \in \{0, 1, 2, 3\}$. The validity of this expression has

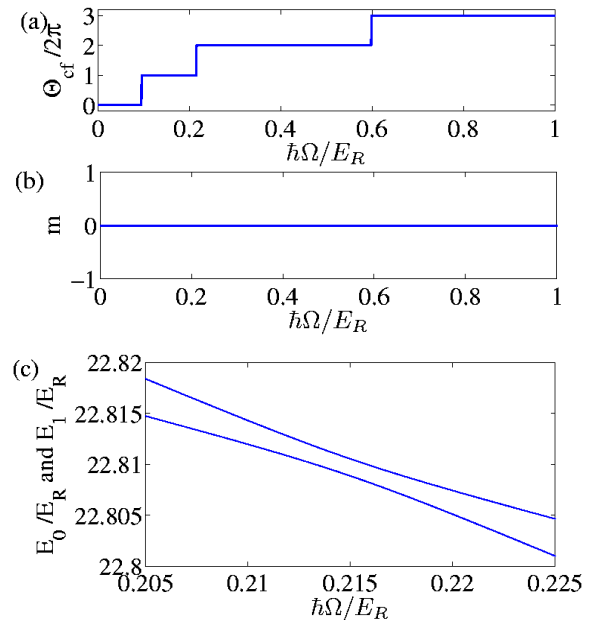


FIG. 12: Four particles in a 4×4 lattice. (a) Number of vortices, $\Theta_{cf}/2\pi$, vs. Ω . Three vortices enter the 4×4 lattice. (b) Quasi-angular momenta, m vs. Ω . The symmetry of the ground state as indicated by the quasi-momentum $m = 0$ does not change even with three vortices entering the system. (c) Zoom-in of lowest two energy levels around the entry of the second vortex shows an avoided energy level crossing. The mixing of states is possible because the ground states on either side have the same discrete rotational symmetry.

been verified both numerically for various lattice sizes and particle numbers and analytically within a Jordan-Wigner transformation approach to hard-core bosons in a ring [36]. Hence, only for odd n does the quasi-angular momentum of the groundstate cycle through all values of m . Cases in which the particle number is commensurate with the four-fold symmetry $n = 4, 8, \dots$ are of particular interest in that these systems always stay in an $m = 0$ state. Note that a simplistic explanation for the validity of Eq. (19) is obtained if all particles occupy a condensate mode with quasi-angular momentum $m = 0, 1, \dots$, yielding a total quasi-angular momentum equal to 0 when $n = 4$.

A. Symmetry-commensurate filling

When the number of particles is commensurate with the four-fold rotational symmetry, the groundstate always has zero quasi-angular momentum. This does not exclude the entry of quantized vortices into the system. To give an example, we analyze the case of four particles in a 4×4 lattice. The largest eigenvalue of the ground state one-body density matrix is found to be $60 - 74\%$

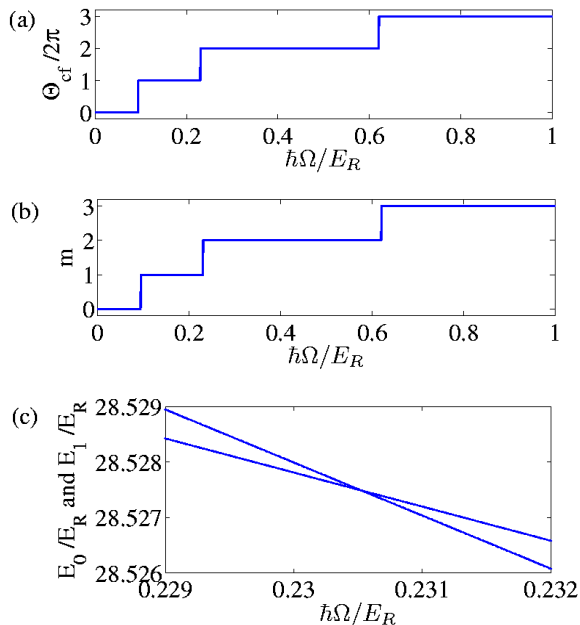


FIG. 13: Five particles in a 4×4 lattice. (a) Number of vortices $\Theta_{cf}/2\pi$ vs. Ω . As before, a maximum of three vortices enter the system (b) Quasi-angular momenta m vs. Ω . Since the filling is incommensurate with the symmetry, the quasi-angular momenta takes on values $m = 0, 1, 2, 3$ (Eq. 19). (c) Zoom-in of lowest two energy levels around the entry of the second vortex shows an energy level crossing as the ground state symmetry changes as a function of a parameter in the Hamiltonian, Ω .

of the total particle number. Since all other eigenvalues are significantly smaller, this number is large enough to refer to the corresponding eigenmode as the condensate wavefunction. The phase winding Θ_{cf} of the condensate wavefunction increases in steps of 2π to a maximum of 6π as the lattice is rotated faster and faster (see Fig. 12(a)). This corresponds to a maximum of $L - 1 = 3$ quantized vortices, with $L \times L$ being the size of the lattice. As in the single particle case, the maximum phase winding that can be observed within a lowest band model is limited by the maximum phase difference of $\pi/2$ between neighbouring sites.

Each vortex entry is associated with an avoided crossing between groundstate and first excited state. This is possible because both states have quasi-angular momentum, $m = 0$, allowing them to mix around the vortex entry point. This is demonstrated in Fig. 12(b) for the entry of the second vortex.

B. Symmetry-incommensurate filling

In behavior similar to that for four particles, the eigenmode corresponding to the condensate wavefunction is macroscopically occupied, and Θ_{cf} for a symmetry-

incommensurate number of particles increases in steps of 2π up to a maximum of $2\pi(L - 1)$. Yet, in contrast with a symmetry-commensurate filling, the discrete rotational symmetry of the system changes with each vortex entry. This is demonstrated in Fig. 13(a) and (b) where we plot both the phase winding and the quasi-angular momentum as a function of Ω for the case of five particles in a 4×4 lattice. In this setting, the maximum phase winding is given by 6π while the quasi-angular momentum takes the values $m = 0, 1, 2, 3$ in accordance with Eq. (19).

Since for symmetry-incommensurate filling the symmetry of the many-body wavefunction is different on either side of the jump in the phase winding, transitions between vortex states cannot occur via the mixing of energy eigenfunctions with the same symmetry. Hence, changes in vorticity are not associated with an avoided crossing between the ground state and the first excited state. Instead, the transition occurs as the energy of an excited state with different quasi-angular momentum and phase winding drops low enough to become the new ground-state. The signature of vortex entry is thus a crossing of energy levels with different discrete rotational symmetry and phase winding. Fig. 13(c) depicts the level crossing associated with the entrance of a second vortex into a system of five particles in a 4×4 lattice. The level crossings are a non-trivial result for many particles since they correspond to a symmetry change in the ground state as a function of a parameter of the Hamiltonian and are indicative of quantum phase transitions [27].

VII. CONCLUSIONS

We have studied zero temperature hard-core bosons in 2D rotating square lattices for filling factors of less than one atom per site using a modified Bose-Hubbard Hamiltonian. An important feature of the system is the quasi-angular momentum, reflecting the discrete rotational symmetry of the lattice. Vortices enter the system as the angular velocity is ramped up. The number of vortices is obtained from the phase winding of the condensate wavefunction around the perimeter of the system. A lattice of size $L \times L$ can contain at most $(L - 1)$ vortices in the lowest band model. We see quantum phase transitions as the quasi-angular momenta of the ground state changes. These are associated with vortices entering a system which has filling incommensurate with the symmetry of the lattice.

Even though we have studied small quantum systems, our work has implications in a broader context. The rotating lattice system is a promising experimental approach allowing one to access more easily the regime of strong quantum-correlations, a major goal in the field in recent years. The novel aspect—the angular rotation frequency of an optical lattice—provides an additional parameter which in principle allows the experimentalist to explore a new axis of phase space.

In order to extend our calculations to study systems

which are of the size which will be more typical in experiments, it is necessary to go beyond the exact quantum ground state calculations. Although this is an important avenue for future work, the basic features of the quantum phase transitions and the emergence of the vortex lattice should persist in larger systems. Here, we have not explored in depth the effects of high rotation which include the fragmentation of the condensate and the emergence of the physics of the fractional quantum Hall effect. In order to access this regime one should go beyond the lowest band description.

VIII. ACKNOWLEDGMENTS

We would like to thank John Cooper, Erich Mueller, Volker Schweikhard, Shih-kuang Tung, Fei Zhou, and Peter Zoller for useful discussions. The authors would like to acknowledge funding support from the Department of Energy, Office of Basic Energy Sciences via the Chemical Sciences, Geosciences, and Biosciences Division (R.B.), the National Science Foundation (B.T.S., L.D.C.), NASA (B.M.P.), and Deutsche Forschungsgemeinschaft (M.K.).

-
- [1] M. R. Matthews, B. P. Anderson, P. C. Haljan, D. S. Hall, C. E. Wieman, and E. A. Cornell, *Phys. Rev. Lett.* **83**, 2498 (1999).
- [2] J. E. Williams and M. J. Holland, *Nature (London)* **401**, 568 (1999).
- [3] K. W. Madison, F. Chevy, W. Wohlleben, and J. Dalibard, *Phys. Rev. Lett.* **84**, 806 (2000).
- [4] P. C. Haljan, I. Coddington, P. Engels, E. A. Cornell, *Phys. Rev. Lett.* **87**, 210403 (2001).
- [5] J. R. Abo-Shaer, C. Raman, J. M. Vogels, and W. Ketterle, *Science* **292**, 476 (2001).
- [6] I. Coddington, P. Engels, V. Schweikhard, and E. A. Cornell, *Phys. Rev. Lett.* **91**, 100402 (2003).
- [7] N. K. Wilkin, and J. M. F. Gunn, *Phys. Rev. Lett.* **84**, 6 (2000).
- [8] B. Paredes, P. Fedichev, J. I. Cirac, and P. Zoller, *Phys. Rev. Lett.* **87**, 010402 (2001).
- [9] U. R. Fischer, P. O. Fedichev, and A. Recati, *J. Phys. B:At. Mol. Opt. Phys.* **37** S301-S310 (2004).
- [10] M. A. Baranov, K. Osterloh, and M. Lewenstein, *Phys. Rev. Lett.* **94**, 070404 (2005).
- [11] V. Schweikhard, I. Coddington, P. Engels, V. P. Mogenendorff, E. A. Cornell, *Phys. Rev. Lett.* **92**, 040404 (2004).
- [12] D. Jaksch, C. Bruder, J. I. Cirac, C. W. Gardiner, and P. Zoller, *Phys. Rev. Lett.* **81**, 3108 (1998).
- [13] M. Greiner, O. Mandel, T. Esslinger, T. W. Hänsch, and I. Bloch, *Nature (London)* **415**, 39 (2002).
- [14] D. Jaksch and P. Zoller, *New J. Phys.* **5**, 56 (2003).
- [15] R. N. Palmer and D. Jaksch, *Phys. Rev. Lett.* **96**, 180407 (2006).
- [16] A. S. Sørensen, E. Demler, and M. D. Lukin, *Phys. Rev. Lett.* **94**, 086803 (2005).
- [17] S. Tung, V. Schweikhard, and E. A. Cornell, *cond-mat/0607697* (2006).
- [18] R. Bhat, M. J. Holland, and L. D. Carr, *Phys. Rev. Lett.* **96**, 060405 (2006).
- [19] C. Wu, H-D. Chen, J-P. Hu, and S-C.Zhang, *Phys. Rev. A* **69**, 043609 (2004).
- [20] J. W. Reijnders and R. A. Duine, *Phys. Rev. A* **71** 063607 (2005).
- [21] A. A. Burkov and E. Demler, *Phys. Rev. Lett.* **96**, 180406 (2006).
- [22] L. D. Landau and S. M. Lifshitz, *Course of Theoretical Physics Vol. 1, Mechanics, Third Edition, Pgs. 126-129* (Butterworth-Heinemann, 1976).
- [23] M. P. A. Fisher, P. B. Weichman, G. Grinstein and D. S. Fisher, *Phys. Rev. B* **40**, 546 (1989).
- [24] W. Zwerger, *J. Opt. B* **5**, S9-S16 (2003).
- [25] L. D. Carr and M. J. Holland, *Phys. Rev. A* **72**, 031604(R) (2005).
- [26] P. Jordan and E. Wigner, *Z. Phys.* **47**, 631 (1928).
- [27] S. Sachdev, *Quantum Phase Transitions* (Cambridge University Press, 2001).
- [28] W. Kohn, *Phys. Rev.* **115**, 14601478 (1959).
- [29] E. I. Blount, *Phys. Rev.* **126**, 16361653 (1962).
- [30] G. H. Wannier, *Rev. Mod. Phys.* **34**, 645655 (1962).
- [31] D. R. Hofstadter, *Phys. Rev. B* **14**, 2239 (1976).
- [32] O. Penrose, and L. Onsager, *Phys. Rev.* **104**, 576 (1956).
- [33] L. Pitaevskii, and S. Stringari, *Bose-Einstein Condensation* (Clarendon Press, Oxford, 2003).
- [34] The lower/upper boundary of the p th Mott zone is obtained by applying the two-state approximation to the p th/ $(p + 1)$ th band, where $p = 1, 2, \dots$ is the band index. The tip of the zone, given by the intersection of the two boundaries, yields a good estimate of the value of t/U at which the superfluid-insulator transition occurs at integer filling.
- [35] N. W. Ashcroft and N. D. Mermin, *Solid State Physics, Pg. 135* (Saunders College Publishing, 1976).
- [36] B. M. Peden, *To be submitted.*